

# Using reinforcement learning to autonomously identify the source of errors for agents in a group mission

Keishu Utimula<sup>1</sup>, Ken-taro Hayaschi<sup>2</sup>, Trevor J. Bihl<sup>3</sup>, Kousuke Nakano<sup>2,4</sup>, Kenta Hongo<sup>5</sup>, Ryo Maezono<sup>2</sup>

<sup>1</sup>*School of Materials Science, JAIST,  
Asahidai 1-1, Nomi, Ishikawa 923-1292, Japan*

<sup>2</sup>*School of Information Science,  
Japan Advanced Institute of Science and Technology (JAIST),  
Asahidai 1-1, Nomi, Ishikawa 923-1292, Japan*

<sup>3</sup>*Air Force Research Laboratory,  
Sensors Directorate, WPAFB, OH 45433, USA*

<sup>4</sup>*International School for Advanced Studies (SISSA),  
Via Bonomea 265, 34136, Trieste, Italy*

<sup>5</sup>*Research Center for Advanced Computing Infrastructure,  
JAIST, Asahidai 1-1, Nomi, Ishikawa 923-1292, Japan and  
\* mwkumk1702@icloud.com  
(Dated: February 11, 2022)*

When agents are swarmed to execute a mission, there is often a sudden failure of some of the agents observed from the command base. Solely relying on the communication between the command base and the concerning agent, it is generally difficult to determine whether the failure is caused by actuators (hypothesis,  $h_a$ ) or sensors (hypothesis,  $h_s$ ). However, by instigating collusion between the agents, we can pinpoint the cause of the failure, that is, for  $h_a$ , we expect to detect corresponding displacements while for  $h_s$  we do not. We recommend that such swarm strategies applied to grasp the situation be autonomously generated by artificial intelligence (AI). Preferable actions (*e.g.*, the collision) for the distinction will be those maximizing the difference between the expected behaviors for each hypothesis, as a value function. Such actions exist, however, only very sparsely in the whole possibilities, for which the conventional search based on gradient methods does not make sense. To mitigate the abovementioned shortcoming, we (successfully) applied the reinforcement learning technique, achieving the maximization of such a sparse value function. Machine learning was concluded autonomously. The colliding action is the basis of distinguishing the hypothesizes. To pinpoint the agent with the actuator error via this action, the agents behave as if they are assisting the malfunctioning one to achieve a given mission.

## I. INTRODUCTION

Cooperative tasks achieved by a group of agents is one of the attractive topics studied in the context of autonomous systems. [1, 2] Because it is likely for each agent to have individual biases in its actuator or sensor performances, it is an important ability for the autonomy to analyze these inherent biases, and to revise the control plan appropriately to continue the group mission. Such biases dynamically vary during the mission with time degradation, sometimes growing up to a failure of some functionality of an agent. To compose proper updates of the plan, the origin of the bias should be identified.

Suppose the command base controlling a group of agents, and the base has detected the bias in the position of an agent (*e.g.*, no change in the  $y$ -direction is observed at all). There are two possible causes for the observed bias, (1) actuator failures (agent not capable to move) and (2) sensor failures (capable to move, but the move not captured). Depending on the hypothesizes [the failure occurs in actuators ( $h_a$ ) or sensors ( $h_s$ )], the updated plan as calibrated by the failure would be quite different. However, because the agent itself is unreliable, it is generally difficult to identify which factor causes the bias only through the communication between the base

and the agent. A quick idea for the identification is to make group actions assisted by other agents, thereby making a collision to the agent with the failure. The collision surely makes the displacement of the agent, which should be detected unless there's sensor failure. In this way, we can identify which hypothesis is correct by planning a group motion. However, such group motions should be designed autonomously by the system (rather than by humans) as a form of 'the strategy to acquire environmental information'. [3]

If we can define proper value functions (say,  $\rho$ ) to measure the ability to capture the distinction between hypothesizes, the proper group motion would be generated to maximize  $\rho$ . Note, however, that among all possible combinations of group actions, such actions with finite  $\rho$  form quite tiny sub-groups; most of the possible actions give  $\rho = 0$ . Namely, the subspaces with finite  $\rho$  exist sparsely in the whole state space (sparse rewards). In such cases, gradient-based optimizations do not work well to propose proper action plans. For such sparse reward optimizations, the reinforcement learning can be used as an effective alternative. This learning has intensively been investigated in the application of autonomous systems. [2, 4–6]

Reinforcement learning [7–9] is forming an established

field, applied to robotics and system-controls. [10, 11] Methodological improvements have intensively been studied especially by verifications on gaming platforms. [12–14] The topic dealt in this research is becoming a subfield entitled as the multi-agent reinforcement learning (MARL). [15–19] As specific examples of multi-agent missions, unmanned aerial vehicles (UAV), [17, 18] sensor resource management (SRM), [18, 20–22] *etc.* are being considered. The problem addressed in this study can also, be regarded as a form of the problems dealing with non-stationary environments for multi-agent reinforcement learning. [23, 24] As time evolves, agents would lose homogeneity as disabilities occur in some of them (thereby becoming heterogeneous.) Coping with such heterogeneity in multiagent reinforcement learning has also been investigated. [15, 17–19, 25] The problem of sparse rewards in reinforcement learning has been recognized and discussed as one of the current challenges in reinforcement learning. [18, 26]

As a prototype of such a problem, we considered a system composed of three agents moving on a  $(x, y)$ -plane administrated by a command base to perform a cooperative task. In performing the task, each agent is asked to convey an item to a goal post individually. The second agent (#2) is assumed to have the actuator failure being incapable to make move along the  $y$ -direction. By giving a quick check with tiny displacements to each agent, the command base can detect the problem existing on #2. However, it may not attribute the cause to the actuators or the sensors. Consequently, the base sets hypothesize,  $h_a$  and  $h_s$ , and starts planning the best cooperative motions to distinguish the hypotheses via reinforcement learning. We observed that the learning that concludes the collision at #2 is the most suitable to recognize a failure situation. Owing to the aforementioned collision, the base could identify that #2 is experiencing problems with its actuators, not the sensors. The base then starts planning the group motions to achieve the conveying task taking into account the disability of #2. We observed that the learning concluding such cooperation is the one where other agents behave as if they assist to compensate the disability of #2 by pushing it toward the goal.

## II. NOTATIONS

Let the state space for the agents be  $\mathbf{R}$ . For instance, for three agents ( $j = 1, 2, 3$ ) on a  $xy$ -plane with each position,  $(x_j, y_j)$ , their state can be specified as  $\mathbf{R} = (x_1, y_1, x_2, y_2, x_3, y_3)$ , that is, the point in the six-dimensional space. The state is driven by a command  $\mathbf{g}$  according the operation plan generated in the command base. When  $\mathbf{g}$  is made for a given  $\mathbf{R}$ , the state is updated depending on which hypothesis  $h_i$  is taken, each of which restricts  $\mathbf{R}$  by individual constraint:

$$\mathbf{g} : \mathbf{R} \rightarrow \tilde{\mathbf{R}}^{(h_i)}(\mathbf{g}, \mathbf{R}) . \quad (1)$$

The difference,

$$D(\mathbf{g}, \mathbf{R}) = \sum_{\langle l, l' \rangle} \|\tilde{\mathbf{R}}^{(h_l)}(\mathbf{g}, \mathbf{R}) - \tilde{\mathbf{R}}^{(h_{l'})}(\mathbf{g}, \mathbf{R})\| , \quad (2)$$

can then be the measure to evaluate the performance, and thereby distinguish the hypothesizes. The best operation plan for the distinction should therefore be determined as

$$\mathbf{g}^* = \arg \max_{\mathbf{g}} D(\mathbf{g}, \mathbf{R}) . \quad (3)$$

The naive idea to perform the optimization using gradient-based methods is unsuccessful because of the sparseness explained in Sec.Introduction; For  $\mathbf{g}$ ,  $D(\mathbf{g}, \mathbf{R}) = 0$ , the gradient is zero for most of  $\mathbf{R}$  because it is incapable of choosing the next update. We, therefore, take reinforcement learning for optimization as an alternative.

Reinforcement learning assumes the value function  $\rho(\mathbf{R}, \mathbf{g})$  which measures the gain by taking the operation  $\mathbf{g}$  for a state  $\mathbf{R}$ . The leaning optimizes such a decision that maximizes not the temporal  $\rho(\mathbf{R}, \mathbf{g})$  but the long-standing benefit,  $Q(\mathbf{R}, \mathbf{g})$ , which is the estimate of accumulative gain for future. The benefit  $Q$  is evaluated in a self-consistent manner (Bellman equation) as, [8]

$$Q(\mathbf{R}, \mathbf{g}) = \rho(\mathbf{R}, \mathbf{g}) + \sum_{\mathbf{R}', \mathbf{g}'} F(\{Q(\mathbf{R}', \mathbf{g}')\}, \{\pi(\mathbf{R}', \mathbf{g}')\}) \quad (4)$$

where the second term sums all possible states ( $\mathbf{R}'$ ) and actions ( $\mathbf{g}'$ ) subsequent to the present choice ( $\mathbf{R}, \mathbf{g}$ ). The function  $F(\{Q(\mathbf{R}', \mathbf{g}')\})$  is composed as a linear combination over  $\{Q(\mathbf{R}', \mathbf{g}')\}$ , representing how the contributions get reduced over time towards future.  $\pi(\mathbf{R}, \mathbf{g})$  appearing in the second term  $F$  describes the policy of taking the next decision  $\mathbf{g}$  at state  $\mathbf{R}$ . As explained in Sec.VII A,  $\pi(\mathbf{R}, \mathbf{g})$  is a probability distribution function with respect to  $\mathbf{g}$ , reflecting the benefit  $Q(\mathbf{R}, \mathbf{g})$  as

$$\pi(\mathbf{R}, \mathbf{g}) = P(Q(\mathbf{R}, \mathbf{g})) .$$

$Q(\mathbf{R}, \mathbf{g})$  is regarded as in Table ( $Q$ -table) with respect to  $\mathbf{R}$  and  $\mathbf{g}$  as rows and columns. At the initial stage, all values on the table are set as random numbers, and updated step by step by the self-consistent iterations as follows: For the random initial values, the temporary decision for initial  $\mathbf{R}_0$  is made formally by

$$\mathbf{g}_0 \sim \pi(\mathbf{R}_0, \mathbf{g}) ,$$

that is the sampling by the random distribution at the initial stage. Given  $\mathbf{g}_0$ , a 'point' ( $\mathbf{R}_0, \mathbf{g}_0$ ) on the  $Q$ -table is updated from the previous random value as

$$Q(\mathbf{R}_0, \mathbf{g}_0) = \rho(\mathbf{R}_0, \mathbf{g}_0) + \sum_{\mathbf{R}', \mathbf{g}'} F(\{Q(\mathbf{R}', \mathbf{g}')\}, \{\pi(\mathbf{R}', \mathbf{g}')\}) \quad (5)$$

where  $\{Q(\mathbf{R}', \mathbf{g}')\}$  referred from the second term is still filled by the random number. The operation  $\mathbf{g}_0$  then promotes the state to  $\mathbf{R}_0 \rightarrow \mathbf{R}_1$ . For the updated  $\mathbf{R}_1$ , similar procedures,

$$\begin{aligned} \mathbf{g}_1 &\sim \pi(\mathbf{R}_1, \mathbf{g}) \\ Q(\mathbf{R}_1, \mathbf{g}_1) &= \rho(\mathbf{R}_1, \mathbf{g}_1) + \sum_{\mathbf{R}', \mathbf{g}'} F(\{Q(\mathbf{R}', \mathbf{g}')\}, \{\pi(\mathbf{R}', \mathbf{g}')\}) \end{aligned}$$

are repeated. As such, the  $Q$ -table is updated in a patchwork manner by the sensible values replacing the initial random numbers. Assisted by the neural-network interpolation, the values for the whole range of the table are filled and then converged by the self-consistent iteration to get the final  $Q$ -table. In the implementation, a user specifies the form of  $\rho(\mathbf{R}, \mathbf{g})$ , and  $F(\{Q(\mathbf{R}', \mathbf{g}')\})$ , providing to the package. In this study, we used the OpenAI Gym [27] package.

Denoting the converged table as  $\bar{Q}(\mathbf{R}, \mathbf{g})$ , we fix the policy as

$$\bar{\pi}(\mathbf{R}, \mathbf{g}) = P(\bar{Q}(\mathbf{R}, \mathbf{g})) , \quad (6)$$

by which we can generate the series of operations to update the state as,

$$\begin{aligned} \bar{g}_0 &\sim \bar{\pi}(\mathbf{R}_0, \mathbf{g}) \\ \bar{g}_0 : \mathbf{R}_0 &\rightarrow \mathbf{R}_1 \\ \bar{g}_1 &\sim \bar{\pi}(\mathbf{R}_1, \mathbf{g}) \\ \bar{g}_1 : \mathbf{R}_1 &\rightarrow \mathbf{R}_2 \\ \dots & \end{aligned} \quad (7)$$

### III. EXPERIMENTS

The workflow to achieve the mission for the agents as described in the last the paragraph in Sec. Introduction is as follows:

- [0a] To examine if there are any errors found in any of the agents, the base issues commands to move each agent by tiny displacements (and consequently #2 is found to have the error).
- [0b] Corresponding to each possible hypothesis ( $h_a$  and  $h_s$ ), the virtual spaces  $\{\mathbf{R}^{(h_i)}\}_{i=a,s}$  are prepared as putting each constraint.
- [1] Reinforcement learning ( $Q_\alpha$ ) is performed at the command base using the virtual space, getting 'the operation plan  $\alpha$ ' designed to distinguish the hypotheses.
- [2] The plan  $\alpha$  is performed by the agents. The command base compares the observed trajectory with trajectory obtained in the virtual spaces in step [1]. By the comparison, the hypothesis giving the closer trajectory to the observed one is identified as what happens ( $h_a$  in this case).
- [3] By taking the virtual space  $\mathbf{R}^{(h_a)}$  as the identified hypothesis, another learning  $Q_\beta$  is performed to get the optimal plan  $\beta$  for the original mission (conveying items to goal posts in this case).
- [4] Agents are operated according to the plan  $\beta$ .

All learnings and operations (as simulation, not by real machines) are performed on a Linux server. The learning part

is the most time-consuming, taking approximately 3h using a single processor without any parallelization to complete. For the learning, we used PPO2 (proximal policy optimization, version2) algorithm [28] implemented on OpenAI Gym [27] library. Reinforcement learning ( $Q_\alpha$ ) is benchmarked on MLP (Multilayer perceptron) and LSTM (long-short time memory) network structures, and the two performances are compared. We did not make any specific tuning for hyperparameters as a default setting, though it has been pointed out that hyperparameter optimization (HPO) can significantly improve the performance of reinforcement learning. [17, 18, 29–33] The comparison shows that MLP performs better (the possible reasons are given in the third paragraph in §IV. As such, the results explained in the main text are obtained by an MLP network structure. Note that, for the agents, LSTM also generates almost similar behaviors as MLP (the possible reasons are given in the appendix, §VII B.

The learning  $Q_\alpha$  seen in step [1] is performed using two virtual spaces,  $V^{(h_s, a)}$ , corresponding to hypotheses,

$$\mathbf{R}^{(h_i)} \in V^{(h_i)} . \quad (8)$$

Each  $\mathbf{R}^{(h_i)}$  can take such possibilities under each constraint of the hypothesis (e.g.,  $y_3$  cannot be updated due to the actuator error). For an operation  $\mathbf{g}$ , the state on each virtual space is updated as

$$\mathbf{g} : \begin{matrix} \mathbf{R}^{(h_s)} \rightarrow \tilde{\mathbf{R}}^{(h_s)} \\ \mathbf{R}^{(h_a)} \rightarrow \tilde{\mathbf{R}}^{(h_a)} \end{matrix} \left( \mathbf{g}, \mathbf{R}^{(h_s)} \right) \left( \mathbf{g}, \mathbf{R}^{(h_a)} \right) . \quad (9)$$

Taking the value function,

$$\rho^{(\alpha)}(\mathbf{g}, \mathbf{R}^{(h_1)}, \mathbf{R}^{(h_2)}) = \left\| \tilde{\mathbf{R}}^{(h_1)}(\mathbf{g}, \mathbf{R}^{(h_1)}) - \tilde{\mathbf{R}}^{(h_2)}(\mathbf{g}, \mathbf{R}^{(h_1)}) \right\| , \quad (10)$$

the two-fold  $Q$ -table is updated self-consistently as

$$\begin{aligned} Q(\mathbf{g}, \mathbf{R}^{(h_1)}, \mathbf{R}^{(h_2)}) &= \rho^{(\alpha)}(\mathbf{g}, \mathbf{R}^{(h_1)}, \mathbf{R}^{(h_2)}) \\ &+ \sum_{\mathbf{g}', \mathbf{R}^{(h_1)}, \mathbf{R}^{(h_2)}} F(\{Q(\mathbf{g}', \mathbf{R}^{(h_1)}, \mathbf{R}^{(h_2)})\}, \{\pi(\mathbf{g}', \mathbf{R}^{(h_1)}, \mathbf{R}^{(h_2)})\}) . \end{aligned}$$

Denoting the converged table as  $\bar{Q}_\alpha(\mathbf{g}, \mathbf{R}^{(h_1)}, \mathbf{R}^{(h_2)})$ , the sequence of operations is obtained as given in Eq.(7), that is,

$$\{\bar{g}_0^{(\alpha)}, \bar{g}_1^{(\alpha)}, \dots, \bar{g}_M^{(\alpha)}\} . \quad (11)$$

The operation sequence generates the two-fold sequence of the (virtual) state evolutions as

$$\{\mathbf{R}_1^{(h_{s,a})} \rightarrow \mathbf{R}_2^{(h_{s,a})} \rightarrow \dots \rightarrow \mathbf{R}_M^{(h_{s,a})}\} , \quad (12)$$

as shown in Fig. 1(a).

In step [2], the agents are operated according to the plan, Eq.(11), to update (real) states as

$$\{\mathbf{R}_1 \rightarrow \mathbf{R}_2 \rightarrow \dots \rightarrow \mathbf{R}_M\} , \quad (13)$$

to be observed by the command base. The base compares Eq. (13) and Eq.(12) to identify whether  $h_s$  or  $h_a$  actually happens ( $h_a$  in this case).

In step [3], the learning  $Q_\beta$  is performed for another value function  $\rho^{(\beta)}$  which earns a higher score when the agents get closer to the goal post (scaling as the inverse of the distance). A big bonus is also earned when they arrive at the goal. The operation sequence is then obtained as

$$\{\bar{g}_{M+1}^{(\beta)}, \bar{g}_{M+2}^{(\beta)}, \dots, \bar{g}_L^{(\beta)}\}, \quad (14)$$

by which the states of the agents are updated as

$$\{R_{M+1} \rightarrow R_{M+2} \rightarrow \dots \rightarrow R_L\}, \quad (15)$$

as shown in Fig. 1(b).

#### IV. DISCUSSIONS

Fig. 1(a) shows two-fold trajectories, Eq. (12), corresponding to the hypotheses,  $h_a$  and  $h_s$ . While  $R^{(h_a)} = R^{(h_s)}$  for the agent #1, the branching  $R^{(h_a)} \neq R^{(h_s)}$  occurs for #2 during the operations. The branching surely earns the score by the value function,  $\rho^{(a)}$  in Eq. (10), implying that the learning  $Q_\alpha$  has properly been performed, thereby the capability of capturing the difference between  $h_a$  and  $h_s$ . The red dotted circle shown in (a) is the collision between #2 and #3, inducing the difference between  $R^{(h_a)}$  and  $R^{(h_s)}$  (note that the trajectories just show the center positions of agents while each agent has a finite radius similar to its size, so the trajectories themselves do not intersect even when the collision occurs). Also, note that the strategy by the collision is never given in a rule-based manner because the agents autonomously deduce their strategy from reinforcement learning.

Three square symbols (closed) located at the edges of a triangle in Fig. 1 are the goalposts for the conveying mission. Fig. 1(b) shows the real trajectories for the mission, where the initial locations of the agents are the final locations of the panel (a). From the initial locations, the agents #1 and #3 immediately arrived at the goals to complete each mission, and departed from the goals heading to the disabled #2 to render assistance. The #2 tried to get closer to its goal using its limited available ability, *i.e.*, the mobility only along the  $x$ -axis. At the closest position, all the agents coalesce and #1 and #3 start assisting to push #2 up towards the goal. Though this behavior is just the consequence of earning more from the value function,  $\rho^{(\beta)}$ , it is interesting that the behavior seems as if agent #1 wants to assist the disabled agent cooperatively. By identifying the constraint  $h_a$  for the agents in learning  $Q_\alpha$ , the consequent learning  $Q_\beta$  is confirmed to generate the optimal operation plans so that the team can earn the best benefit owing to their cooperative behavior as if an autonomous decision has been made by the team.

The performances of LSTM and MLP are compared in terms of the success rate (in percentage) of getting working trajectories to distinguish the hypotheses. Here we note that even when applying the well converged  $Q$ -table, there is some rate required to get non-working trajectories to obtain zero difference between the hypotheses. This is because of the

stochastic nature of the policy, Eq. (6), in generating the trajectories. In the present work, we took 50 independent  $Q$ -tables each of which is generated from scratch, and generated 50 corresponding trajectories. The rate required to obtain capable trajectories to distinguish the hypothesis amounts is 94% for LMS, and 78% for LSTM. In the present comparison, we used the same iteration steps as in  $Q$ -table convergence. Given LSTM has a more complicated internal structure, its learning quality is expected to be relatively lower than LMS for the common condition, thereby the lower performance rate. In other words, a more iteration cost is required for LSTM to achieve the same performance as that of LMS.

For a simulation in a virtual environment space, we need to evaluate the distance between agents at every step. Given this is a pairwise evaluation, its computational cost scales as  $\sim N^2$  for  $N$  agents. This cost scaling can be mitigated by using the domain decomposition method where each agent is evaluated according to its voxel, and the distance between agents is represented by the distance between voxels registered in advance. The corresponding cost scales linearly with  $N$ , at a much faster rate than the naive  $\sim N^2$  evaluation method when the number of agents  $N$  is larger.

#### V. CONCLUSION

Agents performing a group mission can suffer from errors during a mission. We developed multiple hypotheses to investigate the causes of the errors. Cooperative behaviors such as the collision between agents can identify the causes of the errors. We considered autonomous planning of group behaviors via a machine-learning technique. Different hypotheses theorizing the causes of the errors lead to different states to be expected as updated from the same initial state by the same operation. The larger the difference gets, the better its operation plan such that the plan acquires capabilities to distinguish the different hypotheses. In other words, the magnitude of the difference can be the value function to optimize the desired operation plan. Gradient-based optimizations do not work well because a tiny fraction among the vast possible operations (*e.g.*, collisions) can capture the difference, leading to sparse distribution of the finite value for the value function. We discovered that reinforcement learning is the obvious choice to be applied for such problems. The optimal plan concluded by reinforcement learning is the operation that causes the agents to collide with each other. To identify the causes of the errors using this plan, we developed a revised mission plan that incorporates the failure by another learning where the other agents without failure help the disabled agent.

#### VI. ACKNOWLEDGMENTS

The computations in this work have been performed using the facilities of Research Center for Advanced Computing Infrastructure at JAIST. R.M. is grateful for financial support from MEXT-KAKENHI (19H04692 and 16KK0097),

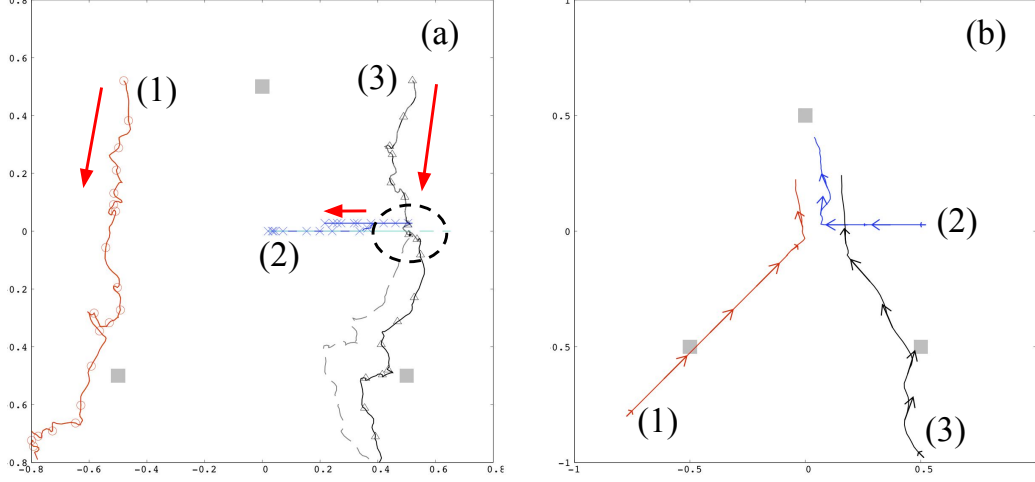


FIG. 1: [realTraj] Trajectories of the agents are driven by each operation plan consequently generated by reinforcement learning [with MLP (Multilayer perceptron) neural network structure],  $Q_\alpha$  first [panel (a)] and  $Q_\beta$  [panel (b)]. The trajectories in (a) are the virtual states,  $\mathbf{R}^{(h_{s,a})}$  (two-fold), branching typically for the agent #2 corresponding to the different hypothesis. Those given in (b) are the real trajectories as given in Eq. (15). The labels, (1) to (3), indicate each agent, which moves along the direction as shown by the red arrows. Dotted circles indicate the collision between agents.

from the Air Force Office of Scientific Research (AFOSR-AOARD/FA2386-17-1-4049;FA2386-19-1-4015).

## VII. APPENDIX

### A. Policy function

Getting the benefit  $Q(\mathbf{R}, g)$ , the most naive choice of the next action would be

$$g^*(\mathbf{R}) = \arg \max_g Q(\mathbf{R}, g), \quad (16)$$

called the greedy method. This is represented in terms of the policy distribution function as

$$\pi(\mathbf{R}, g) = \delta(g - g^*(\mathbf{R})).$$

To express explicitly that  $g^*(\mathbf{R})$  depends on  $Q(\mathbf{R}, g)$  via Eq. (16), let us denote

$$\pi(\mathbf{R}, g) = \delta(g - g^*(Q(\mathbf{R}, g))) = \Delta(Q(\mathbf{R}, g)),$$

as a special case of

$$\pi(\mathbf{R}, g) = P(Q(\mathbf{R}, g)).$$

To enhance the chance to get the optimal solution than the limited exploring by the greedy method in a delta-function wise distribution, there are several choices allowing the finite probability for  $g \neq g^*$ , including ' $\epsilon$ -greedy method',

$P(Q(\mathbf{R}, g)) = (1 - \epsilon) \cdot \Delta(Q(\mathbf{R}, g)) + \epsilon \cdot [\text{RandomNubmer}]$ , or the 'Boltzmann policy',

$$P(Q(\mathbf{R}, g)) = \exp(-\beta Q(\mathbf{R}, g)).$$

### B. Results using LSTM

As explained in main text, the reinforcement learning even using LSTM (long-short time memory) neural network structure also leads to almost the same behaviors for the agents, as shown in Fig. 2, though it achieves less rate to get working trajectories to distinguish hypotheses as explained in main text as well.

[1] H. Lee, H. Kim, and H. J. Kim, IEEE Transactions on Automation Science and Engineering **15**, 189 (2018).

[2] J. Hu, H. Niu, J. Carrasco, B. Lennox, and F. Arvin, IEEE Transactions on Vehicular Technology **69**, 14413 (2020).

[3] K. Friston, Nature Reviews Neuroscience **11**, 127 (2010).

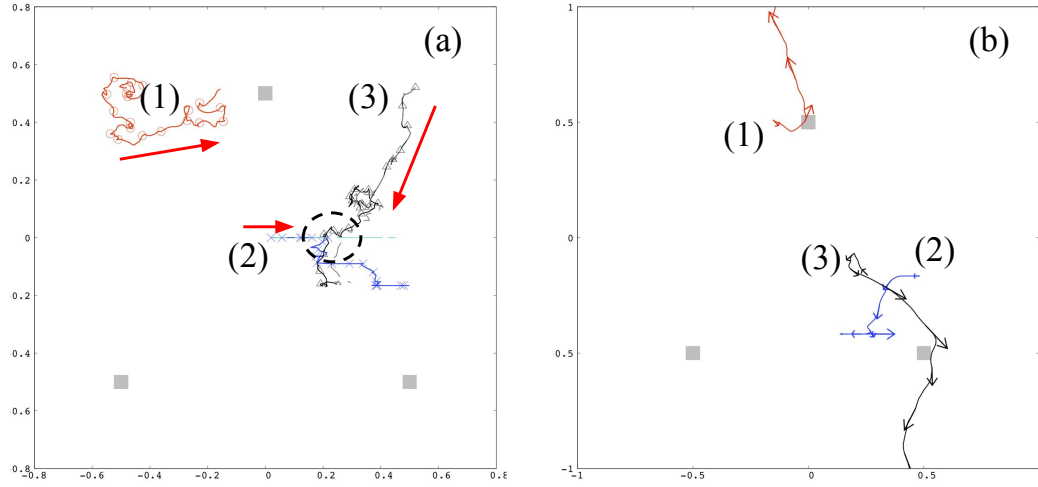


FIG. 2: [realTrajLstm] Trajectories of the agents driven by each operation plan generated by the reinforcement learning [with LSTM (long-short time memory) neural network structure],  $Q_\alpha$  first [panel (a)] and  $Q_\beta$  [panel (b)], consequently. The trajectories in (a) are the virtual states,  $\mathbf{R}^{(h,a)}$  (two-fold), branching typically for the agent #2 corresponding to the different hypothesis. Those given in (b) is the real trajectories as given in Eq. (15). The labels, (1) to (3), indicate each agent, which moves along the direction shown as red arrows. Dotted circles indicate the collision between agents.

- [4] B.-Q. Huang, G.-Y. Cao, and M. Guo, in *2005 International Conference on Machine Learning and Cybernetics*, Vol. 1 (2005) pp. 85–89.
- [5] C. Xia and A. El Kamel, *Robotics and Autonomous Systems* **84**, 1 (2016).
- [6] D. Zhu, T. Li, D. Ho, C. Wang, and M. Q.-H. Meng, in *2018 IEEE International Conference on Robotics and Automation (ICRA)* (2018) pp. 7548–7555.
- [7] O. Nachum, S. Gu, H. Lee, and S. Levine, in *Proceedings of the 32nd International Conference on Neural Information Processing Systems* (2018) pp. 3307–3317.
- [8] R. S. Sutton and A. G. Barto, *Reinforcement Learning: An Introduction*, 2nd ed. (The MIT Press, 2018).
- [9] A. G. Barto, in *The Handbook of Brain Theory and Neural Networks, Second Edition*, edited by M. A. Arbib (The MIT Press, Cambridge, MA, 2002) pp. 963–972.
- [10] X. B. Peng, M. Andrychowicz, W. Zaremba, and P. Abbeel, in *2018 IEEE International Conference on Robotics and Automation (ICRA)* (2018) pp. 3803–3810.
- [11] C. Finn and S. Levine, in *2017 IEEE International Conference on Robotics and Automation (ICRA)* (2017) pp. 2786–2793.
- [12] V. Mnih, K. Kavukcuoglu, D. Silver, A. A. Rusu, J. Veness, M. G. Bellemare, A. Graves, M. Riedmiller, A. K. Fidjeland, G. Ostrovski, S. Petersen, C. Beattie, A. Sadik, I. Antonoglou, H. King, D. Kumaran, D. Wierstra, S. Legg, and D. Hassabis, *Nature* **518**, 529 (2015).
- [13] D. Silver, J. Schrittwieser, K. Simonyan, I. Antonoglou, A. Huang, A. Guez, T. Hubert, L. Baker, M. Lai, A. Bolton, Y. Chen, T. Lillicrap, F. Hui, L. Sifre, G. van den Driessche, T. Graepel, and D. Hassabis, *Nature* **550**, 354 (2017).
- [14] O. Vinyals, I. Babuschkin, W. M. Czarnecki, M. Mathieu, A. Dudzik, J. Chung, D. H. Choi, R. Powell, T. Ewalds, P. Georgiev, J. Oh, D. Horgan, M. Kroiss, I. Danihelka, A. Huang, L. Sifre, T. Cai, J. P. Agapiou, M. Jaderberg, A. S. Vezhnevets, R. Leblond, T. Pohlen, V. Dalibard, D. Budden, Y. Sulsky, J. Molloy, T. L. Paine, C. Gulcehre, Z. Wang, T. Pfaff, Y. Wu, R. Ring, D. Yogatama, D. Wünsch, K. McKinney, O. Smith, T. Schaul, T. Lillicrap, K. Kavukcuoglu, D. Hassabis, C. Apps, and D. Silver, *Nature* **575**, 350 (2019).
- [15] L. Busoniu, R. Babuska, and B. De Schutter, in *2006 9th International Conference on Control, Automation, Robotics and Vision* (2006) pp. 1–6.
- [16] J. K. Gupta, M. Egorov, and M. Kochenderfer, in *Autonomous Agents and Multiagent Systems*, edited by G. Sukthankar and J. A. Rodriguez-Aguilar (Springer International Publishing, Cham, 2017) pp. 66–83.
- [17] K. M. Straub, B. Bonetempo, F. Jones, A. M. Jones, P. Farr, and T. Bihl, *ensor Resource Management using Multi-Agent Reinforcement Learning with Hyperparameter Optimization*, Tech. Rep. (2020) white paper.
- [18] T. Bihl, P. Farr, K. M. Straub, B. Bonetempo, and F. Jones, in *Hawaii International Conference on Systems Sciences 2022* (2020) submitted.
- [19] S. Gronauer and K. Diepold, *Artificial Intelligence Review* (2021), 10.1007/s10462-021-09996-w.
- [20] R. P. Malhotra, M. J. Pribilski, P. A. Toole, and C. Agate, in *Micro- and Nanotechnology Sensors, Systems, and Applications IX*, Vol. 10194, edited by T. George, A. K. Dutta, and M. S. Islam, International Society for Optics and Photonics (SPIE, 2017) pp. 403 – 414.
- [21] R. Malhotra, E. Blasch, and J. Johnson, in *Proceedings of the IEEE 1997 National Aerospace and Electronics Conference. NAECON 1997*, Vol. 2 (1997) pp. 769–776 vol.2.
- [22] A. O. Hero and D. Cochran, *IEEE Sensors Journal* **11**, 3064 (2011).
- [23] T. T. Nguyen, N. D. Nguyen, and S. Nahavandi, *IEEE Transactions on Cybernetics* **50**, 3826 (2020).
- [24] J. Foerster, N. Nardelli, G. Farquhar, T. Afouras, P. H. S. Torr, P. Kohli, and S. Whiteson, in *Proceedings of the 34th International Conference on Machine Learning*, Proceedings of Machine Learning Research, Vol. 70, edited by D. Precup and Y. W. Teh (PMLR, 2017) pp. 1146–1155.

- [25] J. Calvo and I. Dusparic, in *Proc. 26th Irish Conf. Artif. Intell. Cogn. Sci.* (2018) pp. 1–12.
- [26] Z. Wang and M. E. Taylor, in *Proceedings of the Twenty-Sixth International Joint Conference on Artificial Intelligence, IJCAI-17* (2017) pp. 3027–3033.
- [27] G. Brockman, V. Cheung, L. Pettersson, J. Schneider, J. Schulman, J. Tang, and W. Zaremba, “Openai gym,” (2016), arXiv:1606.01540.
- [28] J. Schulman, S. Levine, P. Mortiz, M. Jordan, and P. Abbeel, in *Proceedings of the 32nd International Conference on Machine Learning - Volume 37* (2015) pp. 1889–1897.
- [29] P. Henderson, R. Islam, P. Bachman, J. Pineau, D. Precup, and D. Meger, in *AAAI* (2018).
- [30] T. J. Bihl, J. Schoenbeck, D. Steeneck, and J. Jordan, in *53rd Hawaii International Conference on System Sciences, HICSS 2020, Maui, Hawaii, USA, January 7-10, 2020* (ScholarSpace, 2020) pp. 1–10.
- [31] J. Snoek, H. Larochelle, and R. P. Adams, in *Proceedings of the 25th International Conference on Neural Information Processing Systems - Volume 2* (2012) pp. 2951–2959.
- [32] T. Domhan, J. T. Springenberg, and F. Hutter, in *Proceedings of the 24th International Conference on Artificial Intelligence* (2015) pp. 3460–3468.
- [33] M. T. Young, J. D. Hinkle, R. Kannan, and A. Ramanathan, *Journal of Parallel and Distributed Computing* **139**, 43 (2020).